International Journal of Bifurcation and Chaos, Vol. 6, No. 6 (1996) 1111–1125
Theme Issue (Part 2)

FROM ALMOST PERIODIC TO CHAOTIC: THE FUNDAMENTAL MAP

RAY BROWN
Applied Chaos Technology Corporation,
P.O. Box 1608, Arlington, VA 22210, USA

LEON O. CHUA
Department of Electrical Engineering and Computer Sciences,
University of California, Berkeley, CA 94720, USA

Received December 16, 1995; Revised April 7, 1996

In this paper we present a single map that displays an extraordinary range of dynamics that lies between the Bernoulli maps and almost periodic maps. Of central importance is the fact that this map illustrates how almost-periodic dynamics evolves into Bernoulli dynamics. Due to its continuous spectrum of dynamics between Bernoulli and almost periodic, we call this map the *fundamental map* in contrast to the better known standard map. The range of dynamics found in this map suggests that as order gives way to chaos, both the geometry of the orbit and the sequence of coordinates of the points of the orbit evolve from order to disorder. An interesting point brought out by this map is that the spatial and temporal properties of orbits near each end of the scale bear some striking similarities. Additionally, we show how to derive a Poincaré map from the fundamental map and derive the associated ODE, an equation for an electronic circuit.

1. Introduction

In this paper we describe a one-parameter family of maps that range from a shift on n-symbols to an almost-periodic map. This family illustrates the extraordinary range of dynamics that can occur between these two limits and suggests how the evolution from almost periodic to Bernoulli takes place. A significant question is "Where in this parameter space does chaos actually begin?" The figures obtained from different parameter values of this map illustrate interesting relationships between order and chaos, and how, as order begins to evolve into chaos, the spatial and temporal relationships of an orbit are transformed.

As a practical application, this map may be used to generate data that can be used for the evaluation of empirical tests of pseudo-random processes such as the empty box test [Lake, 1996]. Lastly, we observe that this map may be generalized to higher dimensions.

We begin by showing how to construct a useful formula for a Bernoulli map in two dimensions.

2. From Almost Periodic to Bernoulli

2.1. *A useful formula for a Bernoulli map*

In this section we show how to construct a function of a two-sided Bernoulli map which provides insight into how two-sided Bernoulli maps manifest themselves in algebraic forms. The algebraic representation of two-sided Bernoulli maps is essential to

recognizing when we are encountering chaos in our "everyday" equations. The construction extends the methods used for one-sided shifts found in our paper on examples and counterexamples [Brown & Chua, 1996]. Let

$$\begin{pmatrix} u \\ v \\ w \\ z \end{pmatrix} = \begin{pmatrix} \cos(\phi) \\ \sin(\phi) \\ \cos(\theta) \\ \sin(\theta) \end{pmatrix} \tag{1}$$

Note that while these coordinates are in four dimensions, they are identified by only ϕ and θ, and hence represent only a two-dimensional space embedded in four dimensions.

Now we derive an algebraic representation of a Bernoulli map in terms of elementary functions using the Anosov dynamical system on the torus defined by

$$\mathrm{A}\begin{pmatrix} \phi \\ \theta \end{pmatrix} = \begin{pmatrix} 2\phi + \theta \\ \phi + \theta \end{pmatrix} \bmod (1) \tag{2}$$

This system is also known as the cat map and is known to be a bi-lateral Bernoulli map on the unit square. Note the occurrence of the addition modulo 1 function in this definition of the Anosov map. This must be removed in any algebraic representation we seek because this operation is not an elementary function and it does not occur explicitly in the laws of nature. In fact, the operation of addition mod 1 is a mathematical abstraction that is very useful for proving theorems while obscuring the relationship between the conclusion of a theorem and its connection to the physical world.

By direct substitution of the components of Eq. (2) into Eq. (1), and by an application of the double angle formulas for the sine and cosine, we get, after simplification, the four-dimensional system:

$$\mathrm{T}\begin{pmatrix} u \\ v \\ w \\ z \end{pmatrix} = \begin{pmatrix} 0 & 0 & (u^2 - v^2) & -2uv \\ 0 & 0 & 2uv & (u^2 - v^2) \\ w & -z & 0 & 0 \\ z & w & 0 & 0 \end{pmatrix} \begin{pmatrix} u \\ v \\ w \\ z \end{pmatrix}$$

What is revealed by this map is that the bi-lateral Bernoulli map is equivalent to a map defined by a two-component twist system: the upper right block of four entries is a twist as is the lower left block of four entries. The u, v component of this map is acting as a twist on the w, z component and vice versa.

Implementation of this map on a computer must be done carefully due to the rapid accumulation of round-off errors. By taking the arctangents/ 2π we obtain a map on the unit square which is a bi-lateral Bernoulli map. An implementation of this map in QuickBASIC is:

```
FOR i= 1 TO N
u1=(u^2-v^2)*w-2*u*v*z
v1=2*u*v*w+(u^2-v^2)*z
w1=u*w-v*z
z1=v*w+u*z
phi=arctangent(v1/u1)
theta=arctangent(z1/w1)
u=cos(phi)
v=sin(phi)
w=cos(theta)
z=sin(theta)
PSET (phi/(2*pi),theta/(2*pi)),10
NEXT i
```

The computation of the arctangents is included to compensate for round-off errors. Also, we plot the points in the angular coordinates to retain the uniformity of the Bernoulli distribution.

Following this example we may derive countless additional examples of functions of bilateral shifts on any number of symbols in terms of elementary functions.

2.2. *Combining Bernoulli with almost periodic*

The preceding map, if transformed to complex coordinates $w = \psi_1 + \eta_1 i$, $z = \psi_2 + \eta_2 i$, can be represented by:

$$\mathrm{B}\begin{pmatrix} w \\ z \end{pmatrix} = \begin{pmatrix} w^2 z \\ wz \end{pmatrix} \tag{3}$$

where the modulus of the complex numbers $|w| = |z| = 1$.

An almost-periodic map in complex coordinates can be written as

$$\mathrm{A}\begin{pmatrix} w \\ z \end{pmatrix} = \begin{pmatrix} aw \\ bz \end{pmatrix} \tag{4}$$

where a, b are complex numbers satisfying $|w| = |z| = |a| = |b| = 1$. This is a pair of rotations on the cross product of two unit circles known as the complex torus in two dimensions.

We generalize the Bernoulli map to all two-dimensional complex space by redefining B as

follows:

$$\mathrm{B}\begin{pmatrix} w \\ z \end{pmatrix} = \begin{pmatrix} \dfrac{w^2 z}{|w^2 z|} \\ \dfrac{wz}{|wz|} \end{pmatrix} \tag{5}$$

B is now defined on the complex plane and projects every vector onto the complex torus. The torus is, in effect, an attractor, and B restricted to the torus is an invertible differentiable mapping. It is not necessary to similarly redefine A since A is bounded even when $|w|, |z| \neq 1$.

We form a typical linear combination of these two maps often used in vector computations to get the following map:

$$\mathrm{T}\begin{pmatrix} w \\ z \end{pmatrix} = (1-\lambda)\mathrm{B}\begin{pmatrix} w \\ z \end{pmatrix} + \lambda \mathrm{A}\begin{pmatrix} w \\ z \end{pmatrix} \tag{6}$$

where $0 \leq \lambda \leq 1$. To make this equation a mapping on the torus we need

$$K_1 = |(1-\lambda)w^2 z + \lambda(aw)| \tag{7}$$

and

$$K_2 = |(1-\lambda)wz + \lambda(bz)| \tag{8}$$

We now define the fundamental map as

$$B_\lambda(1, a, b)\begin{pmatrix} w \\ z \end{pmatrix} = \left[(1-\lambda)\begin{pmatrix} \dfrac{w^2 z}{K_1} \\ \dfrac{wz}{K_2} \end{pmatrix} + \lambda \begin{pmatrix} \dfrac{aw}{K_1} \\ \dfrac{bz}{K_2} \end{pmatrix}\right] \tag{9}$$

This is a mapping on the complex torus. When $\lambda = 0$, it is Bernoulli, and when $\lambda = 1$ it is almost periodic. For all other values of λ it is somewhere in-between. Stated differently, it is a one-parameter family of maps, which, except at the origin, are C^∞ (when considered as real valued maps) that continuously vary from an almost-periodic map to a Bernoulli map on two symbols.

We note that B_λ is not an analytic map. This is of no significance since the use of complex coordinates here is only a notational convenience and the theory of complex variables is not used in any of the results. As real valued maps, B_λ and the subsequence maps that we present are infinitely differentiable, except possibly at the origin.

If we generalize this map further we may obtain a set of maps that continuously vary from an almost-periodic map to a Bernoulli map on n-symbols. The generalization is

$$B_\lambda(n, a, b)\begin{pmatrix} w \\ z \end{pmatrix} = \left[(1-\lambda)\begin{pmatrix} \dfrac{w^{n+1} z^n}{K_1} \\ \dfrac{wz}{K_2} \end{pmatrix} + \lambda \begin{pmatrix} \dfrac{aw}{K_1} \\ \dfrac{bz}{K_2} \end{pmatrix}\right] \tag{10}$$

and K_i are the divisors needed to force the mapping to stay on the complex torus.

3. A Poincaré Map: The Second Fundamental Map

In this section we derive a Poincaré map for a circuit which is an arbitrarily small perturbation of the fundamental map and derive the associated circuit equations.

We note that the fundamental map is not always invertible, but by using the technique of Brown & Chua [1993], it can be embedded in an invertible map which is an arbitrarily small perturbation of the fundamental map. This new map, which is a four-dimensional complex map, will be called the second fundamental map. Its key properties are:

(1) it has the full range of dynamics of the fundamental map, ranging from Bernoulli to almost periodic;
(2) it contains period doubling bifurcations to chaos;
(3) it contains the full range of dynamics from attracting dynamics to measure preserving dynamics;
(4) it is invertible; and,
(5) it is a closed form Poincaré map for an electronic circuit.

3.1. *The second fundamental map*

The general method for embedding any map into a Poincaré map was suggested in Brown & Chua [1993] but was not explicitly stated. We now state this result formally:

Theorem 1. *Let $f : \mathbf{R}^n \to \mathbf{R}^n$ be any differentiable (not necessarily invertible) function on $\mathbf{R}^n$. Then f can be embedded in a Poincaré map for an electronic circuit as follows:*

Let $\mathbf{x}, \mathbf{y} \in \mathbf{R}^n$ *be any two vectors in* $\mathbf{R}^n$ *and define* $T: \mathbf{R}^{2n} \to \mathbf{R}^{2n}$ *by the equation:*

$$\mathrm{T}\begin{pmatrix}\mathbf{x}\\ \mathbf{y}\end{pmatrix} = \begin{pmatrix} f(c\mathbf{y}+\mathbf{x}) - c\mathbf{y} \\ c\mathbf{y}+\mathbf{x}\end{pmatrix} \tag{11}$$

where c *is any real number, then,*

(1) T *is* 1-1, *has the same number of derivatives as* f, *and* $\det(\mathrm{DT}) = c^n$;
(2) *for all* $c > 0$ T *is a Poincaré map for an ODE in* $\mathbf{R}^{2n}$;
(3) *for* $c = 0$, *the range of* T *is the graph of* f, *and the orbit of a point* $(\mathbf{x}, \mathbf{y})$ *under* T *is the orbit of* $\mathbf{x}$ *under* f, *i.e.* $(f^{n+1}(\mathbf{x}), f^n(\mathbf{x}))$;
(4) *for any* $\mathbf{x} \in \mathbf{R}^n$, *if* $|c| < 1$ *then* $(f^{n+1}(\mathbf{x}), f^n(\mathbf{x}))$, *is a subset an attractor*;
(5) *as* $c \to 0$, *the attractor of* T *converges to the orbit of* $\mathbf{x}$ *under* f.

Proof. All assertions are direct computations. ■

Using Theorem 1, we write down the second fundamental map:

$$F_\lambda\begin{pmatrix}\Theta\\ \Psi\end{pmatrix} = \begin{pmatrix} B_\lambda(n, c\Psi+\Theta) - c\Psi \\ c\Psi+\Theta\end{pmatrix} \tag{12}$$

From the above theorem we know that the second fundamental map preserves the dynamics of the fundamental map. The analogy is our example of a Poincaré map for a two-dimensional equation which was a small perturbation of the map $x \to 2x \bmod (1)$ in Brown & Chua [1993]. The second fundamental map is the composition of three invertible maps, all of which are time-one maps of complex ODEs. We now show how to construct the circuit using the fundamental map.

3.2. *The circuit*

In this section we use greek letters to represent four-dimensional complex vectors. Thus,

$$\Psi = \begin{pmatrix}u\\ v\end{pmatrix} \qquad \Theta = \begin{pmatrix}w\\ z\end{pmatrix}$$

where u, v, w, z are complex variables. In this notation the fundamental map is written as $B_\lambda(n, \Psi)$. The three components of the second fundamental map are:

$$\mathrm{T}_1\begin{pmatrix}\Theta\\ \Psi\end{pmatrix} = \begin{pmatrix}\Theta\\ c\Psi\end{pmatrix} \tag{13}$$

$$\mathrm{T}_2\begin{pmatrix}\Theta\\ \Psi\end{pmatrix} = \begin{pmatrix}\Theta\\ \Psi+\Theta\end{pmatrix} \tag{14}$$

$$\mathrm{T}_3\begin{pmatrix}\Theta\\ \Psi\end{pmatrix} = \begin{pmatrix}\Theta - \Psi + B_\lambda(n, \Psi)\\ \Psi\end{pmatrix} \tag{15}$$

where c is any real number. The second fundamental map is the composition of these three maps.

The second fundamental map is the Poincaré map for:

$$\begin{pmatrix}\dot\Theta\\ \dot\Psi\end{pmatrix} = \begin{pmatrix} s_3(t)(B_\lambda(n, \Psi) - \Psi) \\ s_2(t)\Theta - s_1(t)\Psi\end{pmatrix} \tag{16}$$

where $s_i(t)$ is a three-phase gate as shown in Fig. 1.

3.3. *Detailed circuit equations*

In this section we write down the eight-dimensional real-variable equations for the second fundamental map circuit. In order to do this we must change our notation, thus in this section we define:

$$\Psi = \begin{pmatrix}x\\ y\\ w\\ z\end{pmatrix} \qquad \Theta = \begin{pmatrix}\theta_1\\ \theta_2\\ \theta_3\\ \theta_4\end{pmatrix}$$

where x, y, w, z, θ_i are *real* variables. In this notation the eight-dimensional circuit equation is

$$\begin{pmatrix}\dot\theta_1\\ \dot\theta_2\\ \dot\theta_3\\ \dot\theta_4\end{pmatrix} = s_3(t)\begin{pmatrix} f_1(x, y, w, z) - c\theta_1 \\ f_2(x, y, w, z) - c\theta_2 \\ f_3(x, y, w, z) - c\theta_3 \\ f_4(x, y, w, z) - c\theta_4\end{pmatrix} \tag{17}$$

$$\begin{pmatrix}\dot x\\ \dot y\\ \dot w\\ \dot z\end{pmatrix} = s_2(t)\begin{pmatrix}\theta_1\\ \theta_2\\ \theta_3\\ \theta_4\end{pmatrix} - s_1(t)\begin{pmatrix}x\\ y\\ w\\ z\end{pmatrix} \tag{18}$$

where we define the f_i in the following equations. First we need to define g_i and K_i as a notational

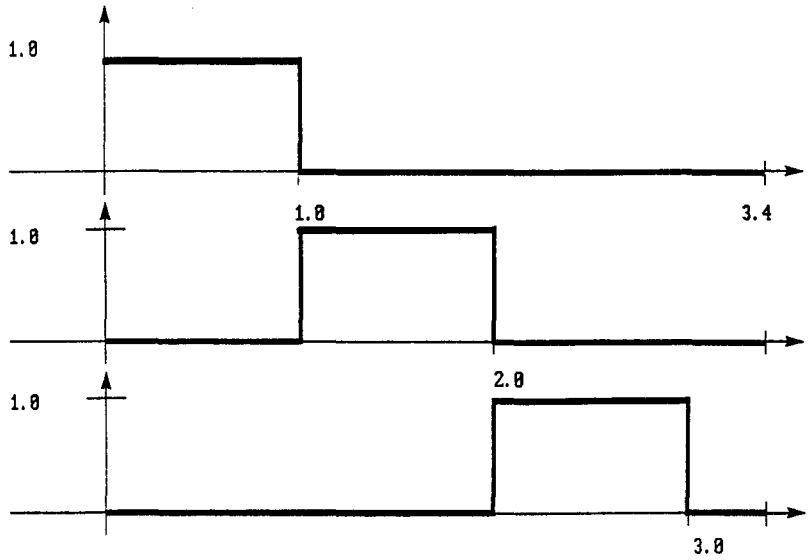

Fig. 1. The functions $s_i(t)$, $i = 1, 2, 3$, constitute a three-phase gate function. Each is periodic of the same period. $s_2(t)$ and $s_3(t)$ are phase shifts of the function $s_1(t)$.

convenience:

$$\begin{pmatrix} g_1(x, y, w, z) \\ g_2(x, y, w, z) \\ g_3(x, y, w, z) \\ g_4(x, y, w, z) \end{pmatrix} = (1-\lambda) \begin{pmatrix} (x^2-y^2)w - 2xyz \\ 2xyw + (x^2-y^2)z \\ xw - yz \\ xz + yw \end{pmatrix} + \lambda \begin{pmatrix} a_1x - a_2y \\ a_2x + a_1y \\ b_1w - b_2z \\ b_2w + b_1z \end{pmatrix} \tag{19}$$

$$K_{1a} = (1-\lambda)^2(x^2+y^2)(w^2+z^2) + \lambda^2(a_1^2 + a_2^2) \tag{20}$$

$$K_{1b} = 2(1-\lambda)\lambda(a_1(xw+yz) + a_2(xz+yw)) \tag{21}$$

and $K_1 = \sqrt{x^2+y^2}\sqrt{K_{1a}+K_{1b}}$.

$$K_2 = \sqrt{(w^2+z^2)[(1-\lambda)^2(x^2+y^2) + \lambda^2(b_1^2+b_2^2) + 2\lambda(1-\lambda)(b_1w+b_2z)]} \tag{22}$$

We can now complete the definition of the functions f_i:

$$f_1 = \frac{g_1}{K_1} \qquad f_2 = \frac{g_2}{K_1} \qquad f_3 = \frac{g_3}{K_2} \qquad f_4 = \frac{g_4}{K_2} \tag{23}$$

3.4. *The attractors*

What is most useful about these maps is what they reveal about the transition between almost periodic and chaotic dynamics. While the second fundamental map is in eight dimensions, the essential dynamics occurs in only two dimensions: In addition to the two dimensions used to portray the dynamics, two more are needed to arrange for the map to operate on a two-dimensional manifold which is compact (the torus). The additional four dimensions are used to make the map invertible. Another way of seeing this is to note that, by inspection, the three component maps that make up the second fundamental map, only one carries the dynamics of the fundamental map, Eq. (18), and that map only uses four dimensions. Of the four dimensions used only two are really needed since the parameter c may be chosen to be arbitrarily small. For example, we could choose $c = 10^{-10000}$.

3.4.1. *Figures 2–11*

In Figs. 2–11 we show how the variation of a single parameter in the second fundamental map produces a diverse array of dynamics which start at Bernoulli and end almost periodic. In Fig. 2, we choose $\lambda = 0$ to obtain a pure Bernoulli orbit. This orbit could be obtained by using the cat map. The orbit appears uniform yet irregular. The map is measure preserving on the attractor. Using the empty box test we would conclude that this orbit is pseudo-random.

In Fig. 3, we have chosen $\lambda = 1$ to obtain a pure almost periodic orbit. This orbit is dense in a closed curve. This orbit could be obtained by a rotation on the torus. Figures 2 and 3 demonstrate the two extremes of the second fundamental map.

In Fig. 4, we choose $\lambda = 0.2$ to obtain a small perturbation of the cat map. The measure preserving feature is apparently lost, but the pseudo-random feature is preserved. This is to be expected due to the "structural stability" of the cat map. We conclude that the map is still chaotic, though not strictly Bernoulli which requires that the map be measure preserving.

In Figs. 5 and 6, we increase λ and the orbits become less uniform and twisted. These images are what we might expect to see if we were to twist the underlying space while leaving the orbit uniform. Another view might be that the two-dimensional orbit has buckled into higher dimensions in order to retain its invertibility.

In Fig. 7, $\lambda = 0.5$ and the orbit now is "half Bernoulli and half almost periodic". A bifurcation has taken place in that repelling regions have appeared as large empty spaces and the orbit is now clearly higher dimensional though we are only showing a two-dimensional projection. Though the map is half and half in the parameter space, it is still clearly chaotic, but not Bernoulli. What we can conclude is that the contribution from the Bernoulli component is still strong enough that the map is chaotic. It is worth recalling at this point that the second fundamental map is a closed form Poincaré map for an electronic circuit.

In Fig. 8, $\lambda = 0.65$ and is weighted toward almost periodic dynamics. The ripples represent the formation of order while the orbit is clearly disorderly to the eye. The Bernoulli component keeps this orbit chaotic. The ripples resemble wind swept sand dunes as seen from overhead. Does this suggest that the ripples in sand dunes are the result of a combined random and almost periodic process?

In Fig. 9, ($\lambda = 0.7$) the addition of 0.05 to the parameter value of Fig. 8 has pushed the orbit into almost-periodic motion. The orbit is an attractor which appears to have chaotic transients. While the dynamics appear almost-periodic, the closed orbits that formed are highly "nonlinear". Thus we have what we might call "geometric chaos" within almost-periodic motion.

In Fig. 10, $\lambda = 0.76$ and the "chaotic" geometry has vanished with another bifurcation. Now the orbit could be described as a uniform almost-periodic motion where we have twisted or wrinkled the underlying space. This apparent uniformity on a twisted space was seen as we perturbed the Bernoulli map in Figs. 4–6.

In Fig. 11, we have a nearly uniform almost-periodic orbit for $\lambda = 0.9$.

Summary of Figs. 2–11

By varying the parameter λ from 0 to 1 we observed the transition from Bernoulli dynamics to almost periodic dynamics. From the initial conditions and rotation factors chosen, we never encountered period doubling bifurcations. By other choices of rotation factors we can obtain period doubling transitions to chaos. One striking feature of the transition is the appearance of the underlying space becoming twisted at each end of the parameter range suggesting that a loss of geometric uniformity may precede the loss of orbit uniformity. During the transition two bifurcations were observed. The first occurred when repelling regions first formed and the second occurred when the attractor became one-dimensional. Clearly, these features are related. In this series of examples, the influence of the Bernoulli term in the second fundamental map maintained the presence of chaos even when the map was weighted toward almost-periodic dynamics. The effect of combining Bernoulli dynamics with almost-periodic dynamics as done here will be more fully explored in *Clarifying Chaos II: Bernoulli Chaos*, to appear.

3.4.2. *Figures 12–27*

In Figs. 12–27 we display a wide range of dynamics that can be found in the second fundamental map. These figures are produced by changing the rotation factor in the almost-periodic term of the fundamental map.

In Fig. 12, $\phi_1 = 0.9$, $\phi_2 = 0$, $\lambda = 0.65$. The system is weighted toward AP, we obtain a one-dimensional attractor with a highly irregular shape.

In Fig. 13, $\phi_1 = 0.5$, $\phi_2 = 0.18$, $\lambda = 0.65$. The orbit is a spiral into a single attracting fixed point.

In Fig. 14, $\phi_1 = 2.5764$, $\phi_2 = 0.4$, $\lambda = 0.60$. The orbit geometry is very complex and the orbit itself appears to be AP. It is an attractor.

In Fig. 15, $\phi_1 = 0.5$, $\phi_2 = 0.5$, $\lambda = 0.80$. The dynamics are AP and if the orbit is sampled over infinite time it will fill out the plane. This is another example of how the orbit geometry begins to bend and twist before chaos sets in.

In Fig. 16, $\phi_1 = 0.5$, $\phi_2 = 0.5$, $\lambda = 0.70$. λ has been shifted toward B and has now become twisted in a higher dimensional space. The nature of the dynamics is uncertain.

In Fig. 17, $\phi_1 = 0.1$, $\phi_2 = 0.1$, $\lambda = 0.64$. An attractor buckled in higher dimensional space appears. The dynamics appear to be chaotic.

In Fig. 18, $\phi_1 = 1.0$, $\phi_2 = 0.1$, $\lambda = 0.705$. This attractor is beyond strange, having both one- and two-dimensional features. The two-dimensional feature is not transient. There is an order to the orbit, but it does not appear to be AP. We might call this class of attractors, X-attractors.

In Fig. 19, $\phi_1 = 0.1$, $\phi_2 = 2.1$, $\lambda = 0.705$. This is another X-attractor having both one- and two-dimensional features. The webbing and the claws are separated by an area that will fill out as the orbit is continued.

In Fig. 20, $\phi_1 = 2.5$, $\phi_2 = 0.1$, $\lambda = 0.635$. Another X-attractor is shown with rope like features extending from the two-dimensional areas.

In Fig. 21, $\phi_1 = 2.6$, $\phi_2 = 0.0$, $\lambda = 0.58$. This attractor is only slightly weighted toward AP. It has folded into higher dimensions as can be seen by the apparent overlapping of the folds. The orbit is clearly chaotic.

In Fig. 22, $\phi_1 = 0.05$, $\phi_2 = 5.5$, $\lambda = 0.73$. This is an orbit that might be chaotic but it cannot be determined by observation. It has areas where points are concentrated. Considered in two dimensions only, it appears not to be an attractor but rather to have areas of nonuniform density.

In Fig. 23, $\phi_1 = 0.7$, $\phi_2 = 2.5$, $\lambda = 0.76$. This orbit is AP with twisted geometry. If the orbit is run out it will fill the plane.

In Fig. 24, $\phi_1 = 2.6$, $\phi_2 = 0.0725$, $\lambda = 0.72$. Another AP orbit with twisted geometry which will fill out the plane.

In Fig. 25, $\phi_1 = 1.0$, $\phi_2 = 0.9$, $\lambda = 0.73$. This AP orbit will fill out the plane and shows relatively moderate twisting.

In Fig. 26, $\phi_1 = 2.6$, $\phi_2 = 0.9$, $\lambda = 0.75$. This orbit has the appearance of being gently twisted. It is AP.

In Fig. 27, $\phi_1 = 0.1$, $\phi_2 = 2.1$, $\lambda = 0.0$. In this figure, we have $c = 0.999$, a value that makes the map nearly measure preserving. The dynamics is indeterminate by observation but the geometry of the orbit looks chaotic. There are areas that appear to be continuous, but this is an illusion. The orbit circulates in higher dimensions taking on the appearance of a ball of yarn that has unraveled in a random manner.

Summary of Figs. 12–27

What is most apparent from these figures is that chaotic dynamics has a far greater diversity than we have supposed. It is clear that we may construct chaotic attractors having high dimensional characteristics and having geometry as bizarre as our imagination allows. It should be clear that chaos is not a low-dimensional phenomena in a measure theoretic sense but can be found in any dimension with any predetermined set of characteristics. The examples constructed here are not merely academic mathematical abstractions, but can be realized in electronic hardware. Additionally, the diversity of attractors constructed from a simple formula have shapes that are suggestive of natural phenomena. This raises the question: "Are many natural processes simple combinations of random and nonrandom processes?", if so, the fundamental map is a simple model for such processes.

3.5. *Figure data*

These figures, computed for $c = 10^{-10}$, are an accurate computer replication of an attractor of the second fundamental map. In only one figure do we allow c to take on a larger value. The resulting figure, Fig. 27, illustrates just how complex the geometry of an orbit can be for the second fundamental map when it is *not* an approximation of the fundamental map.

In Figs. 2–27

$$a = (\cos(\phi_1), \sin(\phi_1)), \quad b = (\cos(\phi_2), \sin(\phi_2)),$$

and $\Psi_0 = \Theta_0$ where

$$\Theta_0 = (\cos(1.266), \sin(1.266), \cos(0.9273), \sin(0.9273))$$

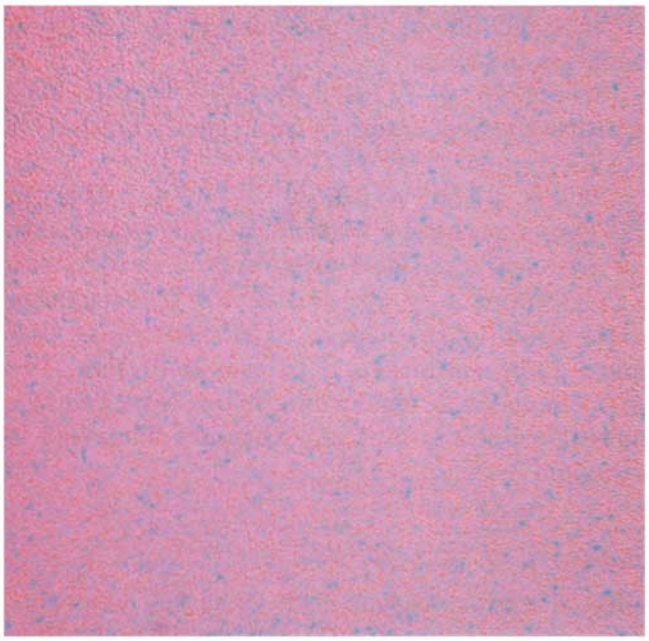

Fig. 2. Orbit of the map $F_0(1, a, b)(w_0, z_0)$ defined by Eq. (12). In this figure, $\phi_1 = 0.9$, $\phi_2 = 0.4$. The horizontal axis is the argument of w, and the vertical axis is the argument of z. This figure shows the upper limits of chaos, a Bernoulli orbit.

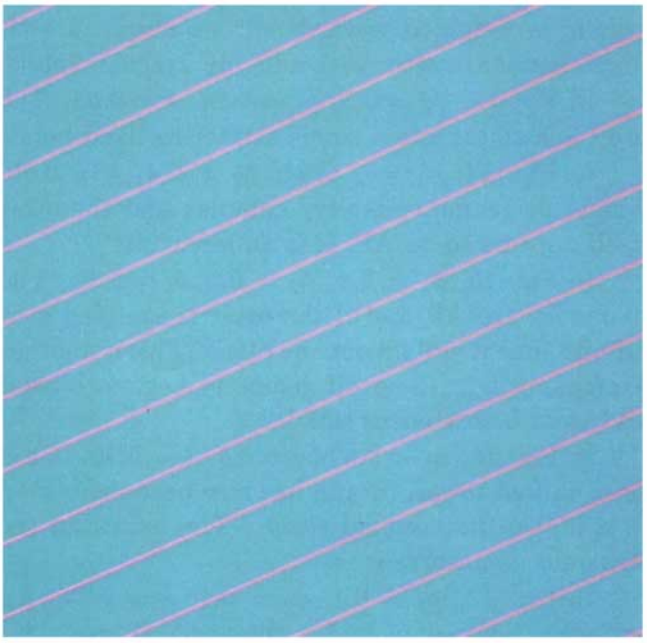

Fig. 3. Orbit of the map $F_1(1, a, b)(w_0, z_0)$ defined by Eq. (12). In this figure, $\phi_1 = 0.9$, $\phi_2 = 0.4$. This figure shows the lower limit of the map's complexity, an almost-periodic orbit that lies on a one-dimensional manifold.

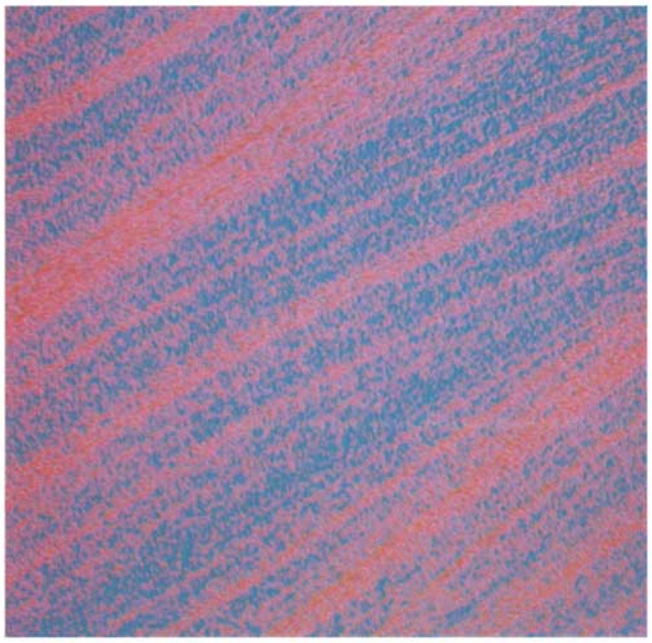

Fig. 4. Orbit of the map $F_{0.2}(1, a, b)(w_0, z_0)$ defined by Eq. (12). In this figure, $\phi_1 = 0.9$, $\phi_2 = 0.4$. We have added a small amount of almost-periodic dynamics to the Bernoulli map causing striations to appear in the previously uniform orbits. The dynamics are still chaotic though apparently not Bernoulli any longer.

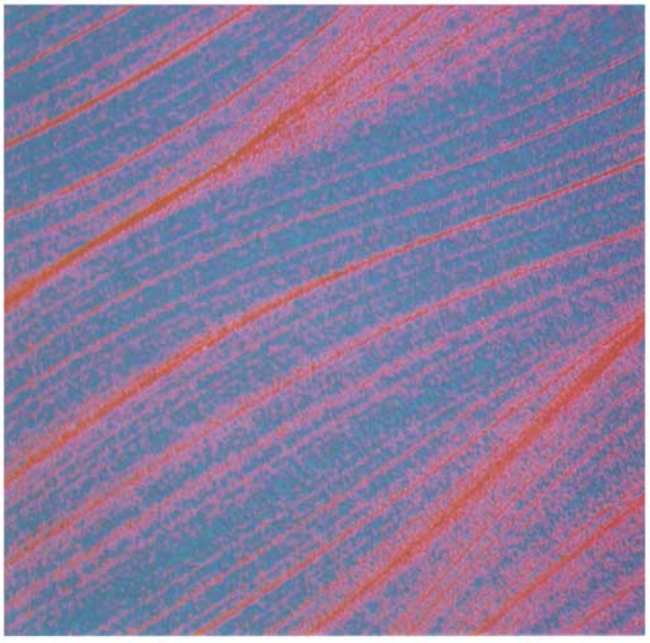

Fig. 5. Orbit of the map $F_{0.3}(1, a, b)(w_0, z_0)$ defined by Eq. (12). In this figure, $\phi_1 = 0.9$, $\phi_2 = 0.4$. By a further increase in almost-periodic dynamics the striations become more prominent. By inspection we determine that chaos is still present.

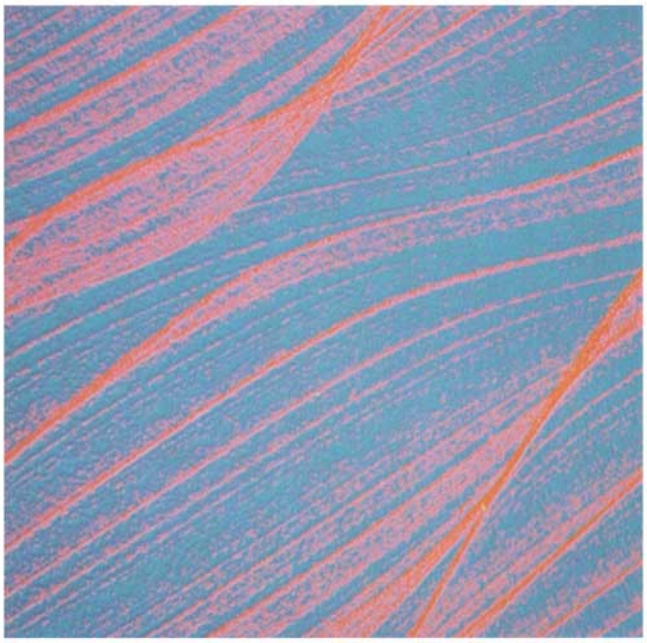

Fig. 6. Orbit of the map $F_{0.4}(1, a, b)(w_0, z_0)$ defined by Eq. (12). In this figure, $\phi_1 = 0.9$, $\phi_2 = 0.4$. Still further increases in almost-periodic dynamics cause the striations to become ever more prominent and by inspection we determine that chaos is still present.

Fig. 7. Orbit of the map $F_{0.5}(1, a, b)(w_0, z_0)$ defined by Eq. (12). In this figure, $\phi_1 = 0.9$, $\phi_2 = 0.4$. Another increment of almost-periodic motion gives a map which is half Bernoulli and half almost-periodic. A bifurcation has taken place as indicated by the prominent empty spaces that have appeared and form repelling regions. The combined mapping remains chaotic.

Fig. 8. Orbit of the map $F_{0.65}(1, a, b)(w_0, z_0)$ defined by Eq. (12). In this figure, $\phi_1 = 0.9$, $\phi_2 = 0.4$. Another increment of almost-periodic motion brings about another bifurcation in that the prominent empty spaces have vanished. The orbit now displays ripples. Order seems to be appearing at this point. The almost-periodic component of the map is now higher than the Bernoulli component, but by inspection we determine that the map is neither Bernoulli nor almost periodic.

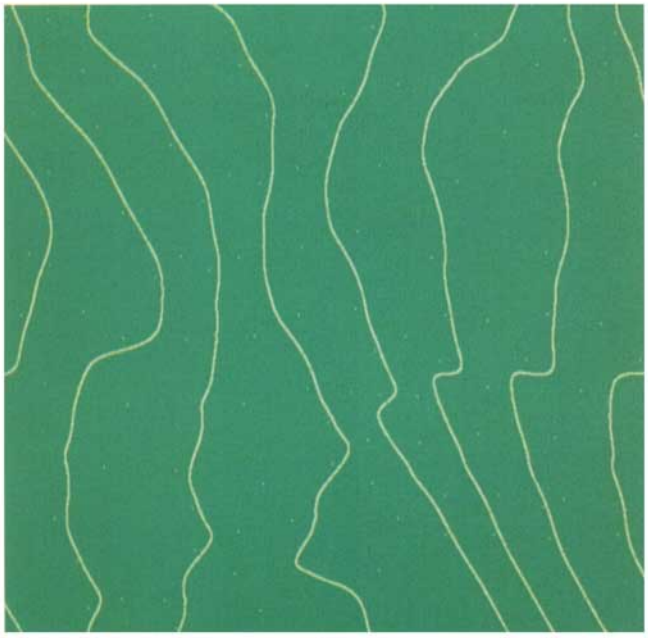

Fig. 9. Orbit of the map $F_{0.7}(1, a, b)(w_0, z_0)$ defined by Eq. (12). In this figure, $\phi_1 = 0.9$, $\phi_2 = 0.4$. A smaller increment of almost-periodic motion brings about another bifurcation: the orbits are one-dimensional attractors and are now clearly almost-periodic.

Fig. 10. Orbit of the map $F_{0.76}(1, a, b)(w_0, z_0)$ defined by Eq. (12). In this figure, $\phi_1 = 0.9$, $\phi_2 = 0.4$. Another small increment of almost-periodic motion brings about another bifurcation: the closure of the orbit is two-dimensional. Something similar to the striations that appeared in Fig. 4 now appear in a more orderly fashion in this figure.

Fig. 11. Orbit of the map $F_{0.9}(1, a, b)(w_0, z_0)$ defined by Eq. (12). As before $\phi_1 = 0.9$, $\phi_2 = 0.4$. The combined map is 90 percent almost-periodic but the dynamics are totally almost-periodic. The striations are lost and the orbit now appears uniform. The closure of the orbit is two-dimensional. In some sense this uniformity is a slight variation of the uniform distribution of points that we associate with a Bernoulli map.

Fig. 12. Orbit of the map $F_{0.65}(1, a, b)(w_0, z_0)$ defined by Eq. (12). In this figure, we change the rotation factor. $\phi_1 = 0.9$, $\phi_2 = 0$. Also, we choose a value of λ which weights the combined map toward almost-periodic dynamics. The dynamics appear almost-periodic but by inspection this is not easy to determine. The attractor is one-dimensional. The geometry of the orbit is becoming complex and is reminiscent of nonlinear dynamics in its curvature.

Fig. 13. Orbit of the map $F_{0.65}(1, a, b)(w_0, z_0)$ defined by Eq. (12). In this figure, the rotation factor is $\phi_1 = 0.5$, $\phi_2 = 0.18$. The dynamics are a simple point attractor.

Fig. 14. Orbit of the map $F_{0.6}(1, a, b)(w_0, z_0)$ defined by Eq. (12). In this figure, the rotation factor is $\phi_1 = 2.5764$, $\phi_2 = 0.4$. The dynamics are indeterminate by inspection and the orbit is another one-dimensional attractor. The geometry of the orbit is very complex.

Fig. 15. Orbit of the map $F_{0.8}(1, a, b)(w_0, z_0)$ defined by Eq. (12). In this figure, the rotation factor is $\phi_1 = 0.5$, $\phi_2 = 0.5$. The dynamics are almost periodic. While the dynamics are simple, the orbit looks as complex as a fingerprint. The closure of the orbit is two-dimensional.

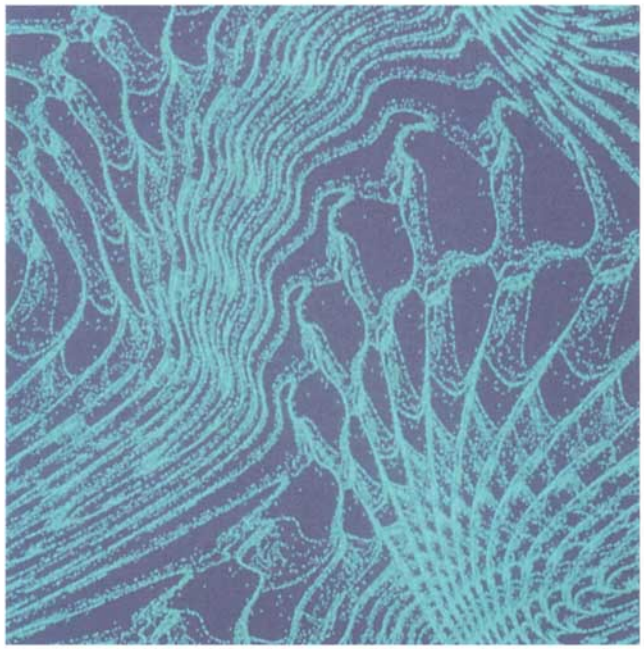

Fig. 16. Orbit of the map $F_{0.7}(1, a, b)(w_0, z_0)$ defined by Eq. (12). In this figure, the rotation factor is $\phi_1 = 0.5$, $\phi_2 = 0.5$. Portions of this attractor bears some resemblance to the top of a sea shell. The dynamics are uncertain but are presumed to be chaotic. The empty regions are repelling regions.

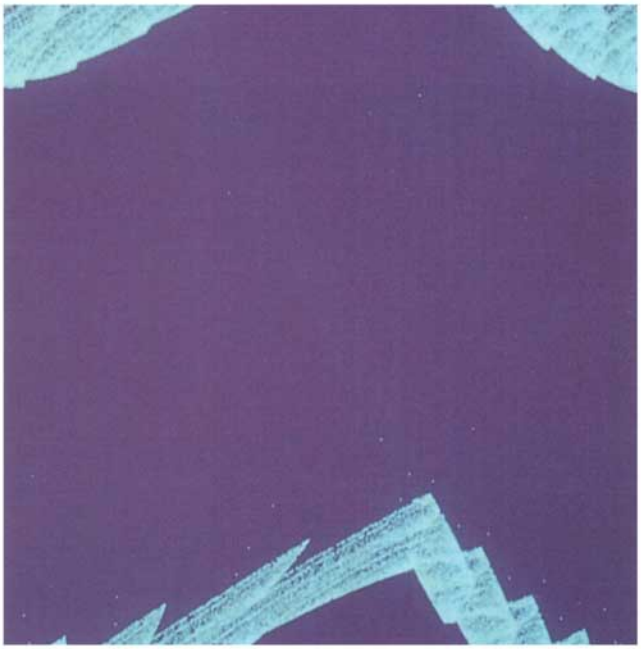

Fig. 17. Orbit of the map $F_{0.64}(1, a, b)(w_0, z_0)$ defined by Eq. (12). In this figure, the rotation factor is $\phi_1 = 0.1$, $\phi_2 = 0.1$. The dynamics are most certainly chaotic. The empty region is repelling.

Fig. 18. Orbit of the map $F_{0.705}(1, a, b)(w_0, z_0)$ defined by Eq. (12). In this figure, the rotation factor is $\phi_1 = 0.1$, $\phi_2 = 0.1$, hence this attractor is a small perturbation of Fig. 17. The dynamics are most certainly chaotic with large empty repelling regions. This attractor seems to be transitioning between one- and two-dimensional dynamics in that neither the one-dimensional portion nor the two-dimensional portion are transients.

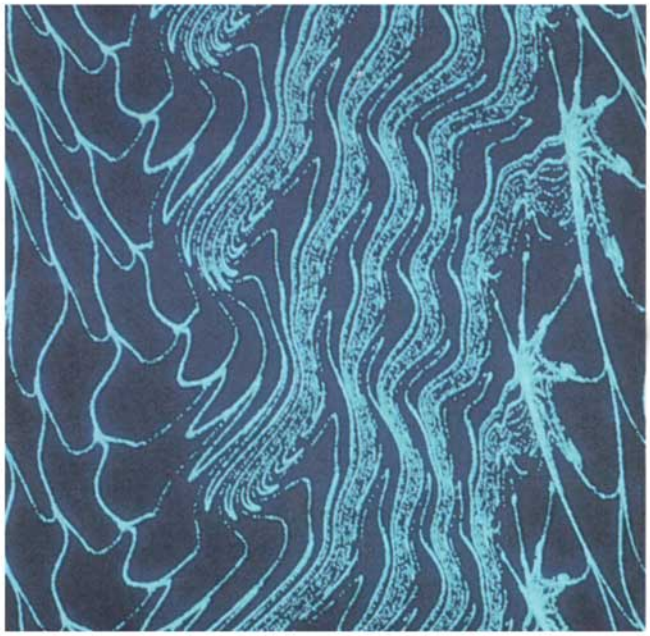

Fig. 19. Orbit of the map $F_{0.705}(1, a, b)(w_0, z_0)$ defined by Eq. (12). In this figure, the rotation factor is $\phi_1 = 0.1$, $\phi_2 = 2.1$. The dynamics are chaotic with large empty repelling regions. Some portions of this attractor resemble the unstable manifold of some two-dimensional twist-and-flip systems. The structures on the right-hand side of the attractor figure resemble cobwebs. They are not transients.

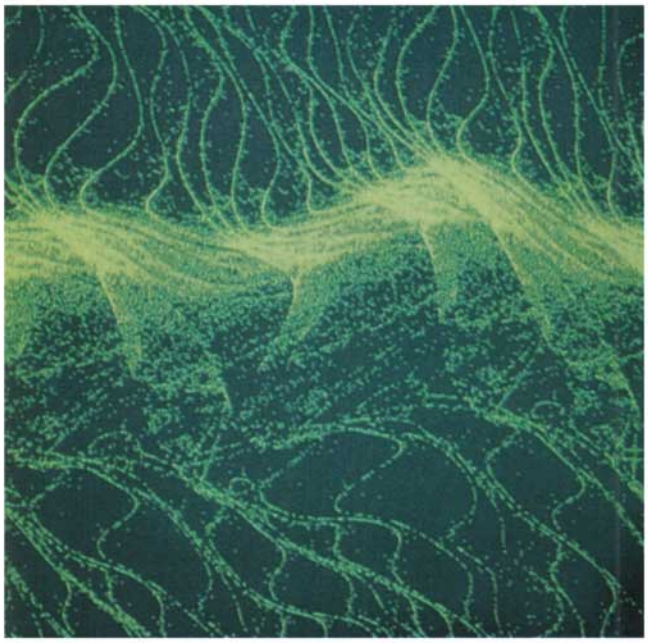

Fig. 20. Orbit of the map $F_{0.635}(1, a, b)(w_0, z_0)$ defined by Eq. (12). In this figure, the rotation factor is $\phi_1 = 2.5$, $\phi_2 = 0.1$. The dynamics are chaotic. Another example of transitioning between one-dimensional and two-dimensional dynamics.

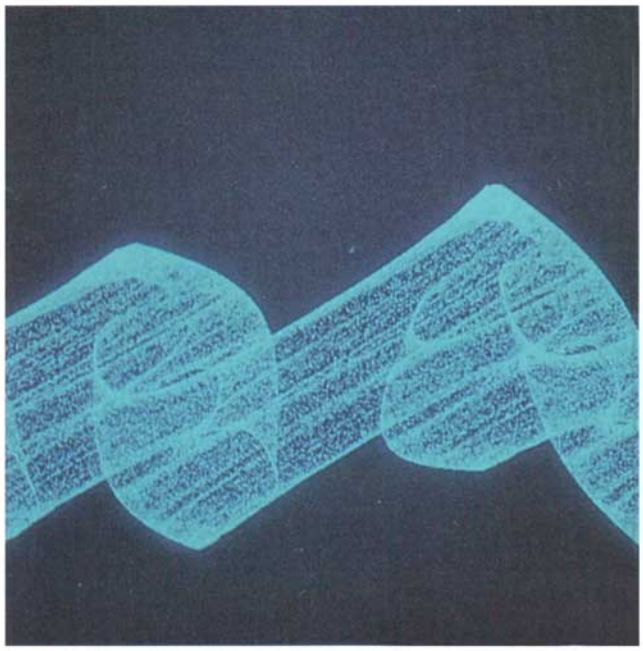

Fig. 21. Orbit of the map $F_{0.58}(1, a, b)(w_0, z_0)$ defined by Eq. (12). In this figure, the rotation factor is $\phi_1 = 2.6$, $\phi_2 = 0.0$. The dynamics are chaotic. This attractor is a small perturbation of Fig. 20 and has transitioned completely to two-dimensional dynamics.

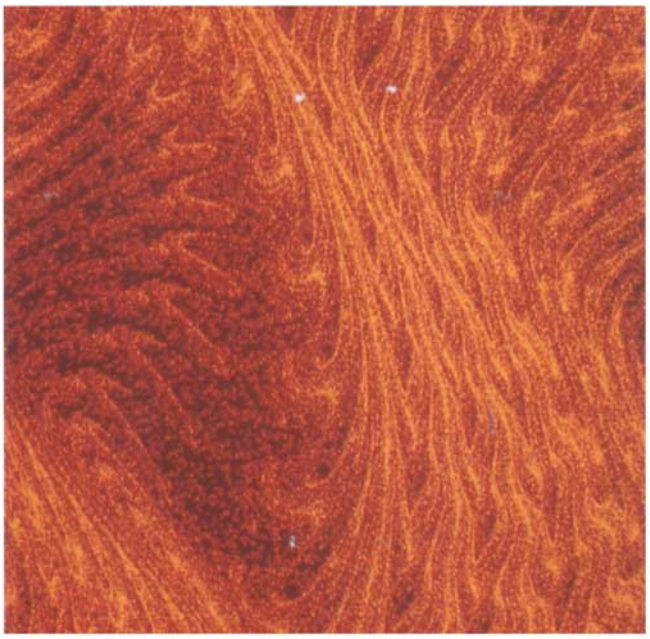

Fig. 22. Orbit of the map $F_{0.73}(1, a, b)(w_0, z_0)$ defined by Eq. (12). In this figure, the rotation factor is $\phi_1 = 0.5$, $\phi_2 = 5.5$. The dynamics are chaotic. The feathery texture of this attractor gives it the appearance of smoke.

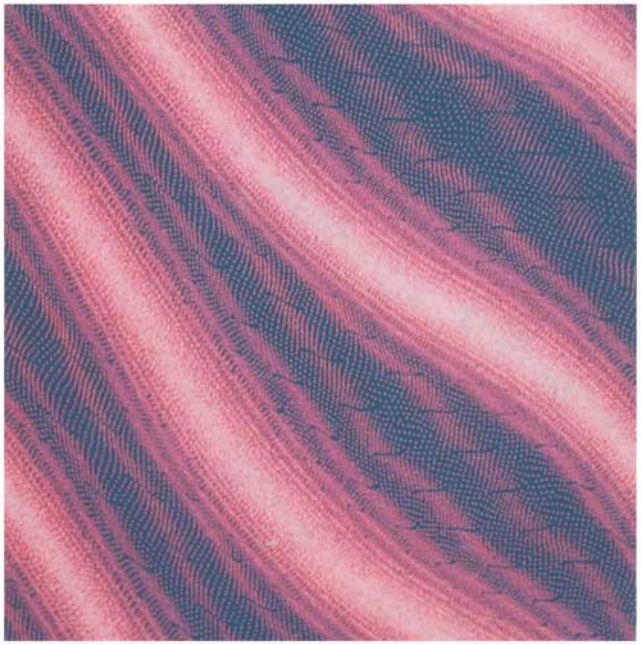

Fig. 23. Orbit of the map $F_{0.76}(1, a, b)(w_0, z_0)$ defined by Eq. (12). In this figure, the rotation factor is $\phi_1 = 0.7$, $\phi_2 = 2.5$. The dynamics are almost periodic. This attractor could also resemble some portions of a smoke trail.

Fig. 24. Orbit of the map $F_{0.72}(1, a, b)(w_0, z_0)$ defined by Eq. (12). In this figure, the rotation factor is $\phi_1 = 0.0725$, $\phi_2 = 2.6$. The dynamics are uncertain. This attractor resembles the surface of a large body of water blown by a high wind as seen from above.

Fig. 25. Orbit of the map $F_{0.73}(1, a, b)(w_0, z_0)$ defined by Eq. (12). In this figure, the rotation factor is $\phi_1 = 1.0$, $\phi_2 = 0.9$. The dynamics are almost periodic. This attractor also resembles the surface of a large body of water blown by a high wind as seen from above.

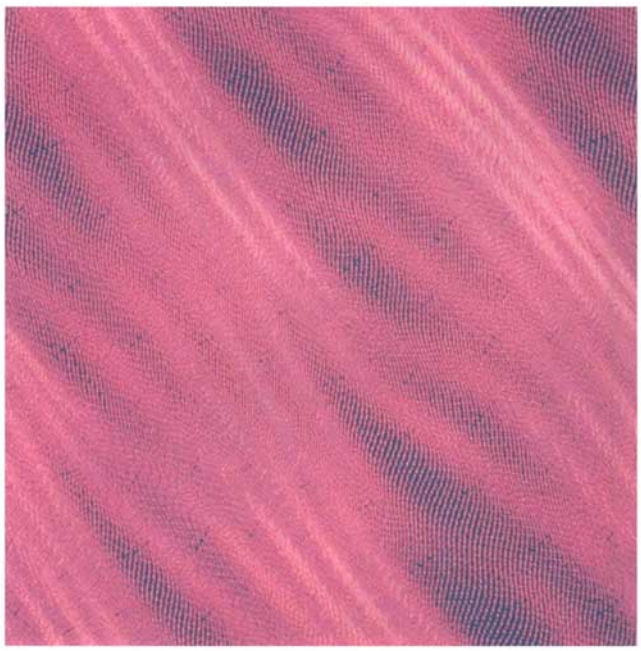

Fig. 26. Orbit of the map $F_{0.75}(1, a, b)(w_0, z_0)$ defined by Eq. (12). In this figure, the rotation factor is $\phi_1 = 2.6$, $\phi_2 = 0.9$. The dynamics are almost periodic. This attractor resembles the surface of a thick liquid or pliable solid such as taffy.

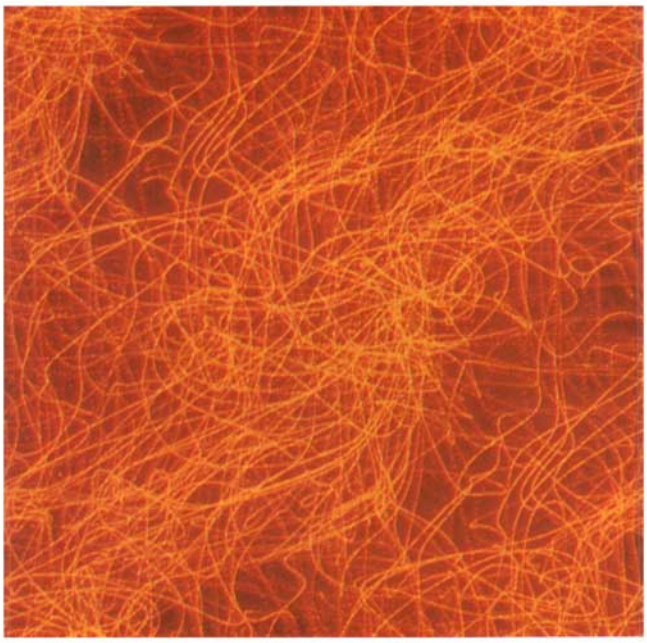

Fig. 27. Orbit of the map $F_{0.75}(1, a, b)(w_0, z_0)$ defined by Eq. (12) where $c = 0.999$. The dynamics are very nearly measure-preserving. In this figure, the rotation factor is $\phi_1 = 0.1$, $\phi_2 = 2.1$. The dynamics are uncertain. This attractor resembles a tangled ball of yarn.

The graph coordinates, (x, y), are the argument of the first component of the complex vector $F_\lambda(1, a, b)(\Theta, \Psi)$, i.e., Θ. The length of the x-axis and y-axis is 6.5. The orbits all lie in a square with sides of length 2π.

4. Summary and Conclusions

The fundamental map describes an extraordinary range of two-dimensional dynamics. It is particularly useful in developing intuition into the evolution from almost-periodic dynamics to the highest end of chaotic dynamics, the Bernoulli maps. On each end of this dynamical spectrum analogous changes take place as we move toward the other end of the spectrum in that the orbit geometry first loses its uniformity. Further, as we proceed from almost-periodic dynamics toward Bernoulli the map becomes more nonlinear and this nonlinearity first appears as a change in the geometric appearance of the orbits. These changes can be used to better understand the transition into chaos and to discriminate between chaotic and non-chaotic processes. In particular, tests for randomness can be examined by the use of data generated by the fundamental map. The fundamental map may be useful in identifying the point of demarcation between chaos and order. Lastly, the fundamental map may be a simple model for how random and non-random processes combine to form complex and varied natural processes.

Acknowledgments

The work of the first author was supported by ONR contract N00014-95-C-0153.

References

Arnold, V. & Avez, A. [1989] *Ergodic Problems of Classical Mechanics* (Addison-Wesley, New York).

Beardon, A. [1991] *Iteration of Rational Functions* (Springer-Verlag, New York).

Brown, R. & Chua, L. [1993] "Dynamical synthesis of Poincaré maps," *Int. J. of Bifurcation and Chaos* **3**(5), 1235–1267.

Brown, R. & Chua, L. [1996] "Clarifying chaos: Examples and counterexamples," *Int. J. of Bifurcation and Chaos* **6**(2), 219–249.

Cornfeld, I., Fomin, S. & Sinai, Y. [1982] *Ergodic Theory* (Springer-Verlag, Berlin).

Katznelson, Y. [1976] *An Introduction to Harmonic Analysis* (Dover Publications, New York).

Lake, D. E. [1996], "Detecting regularity in minefields and chaotic signals using the empty box test," *Proceedings of the 8th IEEE Signal Processing Workshop on Statistical Signal and Array Processing* Corfu, Greece, June 24–26, 1996 (to appear).

Shil'nikov, L. [1994] "Chua's circuit: Rigorous results and future problems," *Int. J. of Bifurcation and Chaos* 4(3), 489–519.

Walters, P. [1982] *Introduction to Ergodic Theory* (Springer-Verlag, New York).

Wiggins, S. [1990] *Introduction to Applied Nonlinear Dynamical Systems and Chaos* (Springer-Verlag, New York).

Wiggins, S. [1992] *Chaotic Transport in Dynamical Systems* (Springer-Verlag, New York).